

# An influence of the spectator-nuclear motion on nonresonant formation of the muonic hydrogen molecules

Andrzej Adamczak\*

*Institute of Nuclear Physics Polish Academy of Sciences,  
Radzikowskiego 152, PL-31342 Kraków, Poland*

Mark P. Faifman†

*National Research Centre Kurchatov Institute,  
pl. Akademika Kurchatova 1, 123182 Moscow, Russia*

(Dated: November 23, 2021)

## Abstract

A model for description of nonresonant formation of the muonic molecules in collisions of the muonic hydrogen atoms with the hydrogenic molecules has been developed with taking into account the internal motion of all nuclei. It has been shown that such a motion leads to a significant smearing of the calculated energy-dependent formation rates at low collision energies. In particular, this effect is strong in the  $dd\mu$  and  $dt\mu$  formation. An appreciable isotopic effect in the case of nonresonant  $dd\mu$  formation in  $d\mu$  collisions with the molecules  $D_2$  and  $HD$  has been found. All these effects are of importance for many experimental researches in low-energy muon physics.

PACS numbers: 36.10Ee, 34.50.-s

---

\* andrzej.adamczak@ifj.edu.pl

† faifmark@gmail.com

## I. INTRODUCTION

The formation of muonic molecules is one of crucial links in the chain of physical processes caused by the negative  $\mu^-$  muons in a hydrogen isotope mixtures (see reviews [1–3] and references therein). The interpretation and analysis of the data obtained in various experiments with low-energy muons require a knowledge of the energy-dependent formation rates of various muonic hydrogen molecules. For example, in the studies of muon-catalyzed  $pt$  and  $tt$  fusion [4, 5], in the PSI measurements [6, 7] of the muon capture in the hydrogen-isotope nuclei, as well as in the planned determination of the Zemach radius of proton by the FAMU collaboration [8] at RAL and by the CREMA collaboration [9] at PSI.

The muonic molecule being the three-body system (ion, in reality) consists of the two hydrogen isotope nuclei and the muon. Such  $\mu$ -molecular systems are formed in collisions of the muonic  $a\mu$ -atoms ( $a = p, d$ , or  $t$ ) with the hydrogen-isotope (hydrogenic) molecules  $BX$  ( $B, X = \text{H, D, or T}$ ). The quantum states of formed muonic molecules are defined by the different rotational ( $J$ ) and vibrational ( $v$ ) quantum numbers (see Table I)<sup>1</sup>.

TABLE I. The binding energies  $|\varepsilon_{Jv}|$  (in eV) of the muonic molecules  $ab\mu$  in the states  $(Jv)$ .

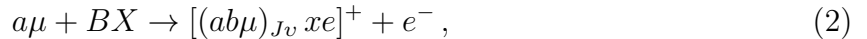
State	Molecule					
$(Jv)$	$pp\mu$	$pd\mu$	$pt\mu$	$dd\mu$	$dt\mu$	$tt\mu$
(11)	—	—	—	1.965	0.631	45.206
(30)	—	—	—	—	—	48.838
(01)	—	—	—	35.844	34.834	83.771
(20)	—	—	—	86.494	102.649	172.702
(10)	107.266	97.498	99.126	226.682	232.471	289.142
(00)	253.152	221.549	213.840	325.074	319.140	362.910

The loosely bound ( $J = 1, v = 1$ ) states of the  $dd\mu$  and  $dt\mu$  molecules refer to the formation, as a rule, by the resonance mechanism [13] in the reaction of following type



where the released energy of about  $|\varepsilon_{11}|$  is transferred to the excitation of rotational-vibrational states ( $K\nu$ ) of the molecular complex  $[(dt\mu)_{11} dee]$ . The rates  $\lambda_{dt\mu}$  and  $\lambda_{dd\mu}$  of such resonance reactions depend on the target temperature  $T$ . For the room temperature  $T = 300$  K, these rates are on the order of  $10^8 \text{ s}^{-1}$  [2] and  $10^6 \text{ s}^{-1}$  [3, 14], respectively.

In any other state ( $Jv$ ), the muonic molecular ions  $ab\mu$  are formed via the nonresonant process [1, 15, 16]



with conversion of the released energy into electron ionization of the  $BX$  molecule. The rates of transitions (2) to all ( $Jv$ )-states of  $ab\mu$  have been calculated in Ref. [17], except that for the ( $J = 1, v = 1$ ) states of the molecules  $dd\mu$  and  $dt\mu$ . Later on, the nonresonant formation in such a loosely bound state was also considered for collision energies higher

<sup>1</sup> The table is compiled from the data of Ref. [10], whereas the binding energies of the state ( $J = 1, v = 1$ ) are taken from Ref. [11] (see also Ref. [12]).

than the electron ionization potential of the  $BX$  molecule [18]. There was shown that the corresponding rates of reactions (2) could be significant. The rates of such nonresonant formation reach the magnitudes up to  $10^7 \text{ s}^{-1}$ , depending on energy of  $a\mu$  collision with a  $BX$  molecule.

A comparison of the measured [3, 19, 20] and calculated [17, 18] rates of nonresonant transitions in reactions (2) demonstrated a very good agreement for different muonic molecules, although some differences between the theory and experiments were observed in the case of low-temperature H/D targets. In order to improve the calculating scheme [17], in which the distance between the center of mass (CM) of molecule  $ab\mu$  and the spectator nucleus  $x$  of the molecule  $BX$  was kept constant, the internal motion of both the nuclei  $b$  and  $x$  within the  $BX$  molecule is taken into account in the present work.

In Sec. II, a transformation of the nonresonant formation rates calculated [17] in the center of mass of the  $a\mu + b$  system to the laboratory system  $a\mu + BX$  is carried out with taking into account the internal motion of nuclei  $b$  and  $x$  within the molecule  $BC$ . A harmonic model of the molecular vibrations is used in Sec. III in order quantitatively to describe the internal nuclear motion within the hydrogenic molecules. The results and discussion are included in Sec. IV.

## II. TRANSFORMATION OF THE NONRESONANT FORMATION RATES BETWEEN THE CENTER-OF-MASS AND LABORATORY SYSTEMS

The rates  $\lambda$  of nonresonant formation of  $ab\mu$  molecules were calculated in Ref. [17] assuming that the nucleus  $x$  in the molecule  $BX$  is a distant spectator, which is located at a fixed position  $\mathbf{R}_0$  with respect to the nucleus  $b$  (see Fig. 1). These rates, which were calculated in

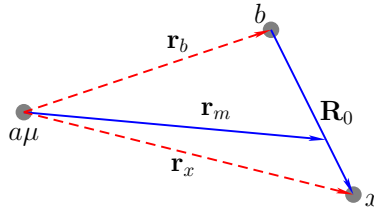


FIG. 1. (Color online) Relative coordinates for the description of nonresonant formation of the  $ab\mu$  molecule in  $a\mu$  collision with molecule  $BX$ . The electrons are not displayed here. Vector  $\mathbf{r}_m$  denotes the position of the  $BX$  molecule center of mass reckoned from the  $a\mu$  atom center of mass.

the center of mass of the  $a\mu + b$  system (*nuclear CMS*), are functions of collision energy  $\varepsilon$  in this system:  $\lambda = \lambda(\varepsilon)$ . A dependence of  $\varepsilon$  on the momentum  $\mathbf{k}$  of relative motion of the  $a\mu$  atom and the nucleus  $b$  is expressed as follows

$$\varepsilon = \frac{\mathbf{k}^2}{2\mu}, \quad \mathbf{k} = \mu \frac{d\mathbf{r}_b}{dt}, \quad (3)$$

where the reduced mass  $\mu$  of the  $a\mu + b$  system is given by the relations

$$\mu^{-1} = M_{a\mu}^{-1} + M_b^{-1}, \quad M_{a\mu} = M_a + M_\mu, \quad (4)$$

in which  $M_\mu$  is the muon mass and the masses of nuclei  $a$  and  $b$  are denoted by  $M_a$  and  $M_b$ , respectively.

For the analysis of the experimental data, it is often more convenient to use the formation rates as functions of kinetic energy  $E$  of the  $a\mu$  atoms in the laboratory frame (LAB). Such LAB rates were estimated in Refs. [18, 21] using the rates  $\lambda(\varepsilon)$ , which were calculated in the nuclear CMS, and the transformation of the following form [22, 23]:

$$\lambda(E, T) = \int_0^\infty \lambda(\tilde{\varepsilon}_Q) G(\mathbf{p}, \tilde{\varepsilon}_Q) d\tilde{\varepsilon}_Q, \quad (5)$$

with the “distribution function”  $G(\mathbf{p}, \varepsilon_Q)$  defined below

$$G(\mathbf{p}, \varepsilon_Q) = \sqrt{\frac{M_{bx}}{2\pi T} \frac{M_{a\mu}}{\mu_t p}} \left\{ \exp \left[ -\frac{M_{bx}}{2T} \left( \frac{Q}{\mu_t} - \frac{p}{M_{a\mu}} \right)^2 \right] - \exp \left[ -\frac{M_{bx}}{2T} \left( \frac{Q}{\mu_t} + \frac{p}{M_{a\mu}} \right)^2 \right] \right\}. \quad (6)$$

The total mass  $M_t$  and the reduced mass  $\mu_t$  of the  $a\mu + BX$  system (henceforth called the *molecular* system) are given by the relations

$$M_t = M_{a\mu} + M_{bx}, \quad \mu_t^{-1} = M_{a\mu}^{-1} + M_{bx}^{-1}, \quad (7)$$

$$M_{bx} = M_b + M_x,$$

where  $M_x$  denotes the mass of nucleus  $x$ . In Eqs. (5)–(6), the momentum  $\mathbf{p}$  of  $a\mu$  atom in LAB and the momentum  $\mathbf{Q}$  of relative motion of the  $a\mu$  atom and molecule  $BX$  are related to the corresponding kinetic energies  $E$  and  $\varepsilon_Q$  by the following expressions:

$$E = \mathbf{p}^2 / (2M_{a\mu}) \quad (8)$$

and

$$\varepsilon_Q = \frac{\mathbf{Q}^2}{2\mu_t}, \quad \mathbf{Q} = \mu_t \frac{d\mathbf{r}_m}{dt}. \quad (9)$$

The employment of Eqs. (5)–(9) for calculating the formation rates was based on the assumption that the target molecules  $BX$  are point-like objects and their kinetic-energy distribution in a target at temperature  $T$  has the Maxwellian shape. The dependencies

$$\varepsilon_Q = \frac{\mu_t}{\mu} \varepsilon, \quad \mathbf{Q} = \frac{\mu_t}{\mu} \mathbf{k} \quad (10)$$

between the relative energies  $\varepsilon_Q$  and  $\varepsilon$ , as well as between the corresponding momenta  $\mathbf{Q}$  and  $\mathbf{k}$ , are inferred from Eqs. (3) and (9) using the approximation  $\mathbf{r}_m \approx \mathbf{r}_b$ .

The simplified procedure of the formation-rate transformation between the *nuclear* (or *molecular*) CMS and LAB, which is briefly described above, denotes in fact that the internal motion of the nuclei in a target molecule  $BX$  is neglected and that merely the correct masses  $M_{bx}$  and  $\mu_t$  of the system  $a\mu + BX$ , which are defined in Eq. (7), are substituted in Eqs. (5)–(8) instead of the masses  $M_b$  and  $\mu$  of the system  $a\mu + b$  [from Eq (4)].

Since the hydrogenic molecules are very light, the kinetic energy  $\varepsilon_q$

$$\varepsilon_q = \frac{\mathbf{q}^2}{2\mu_{bx}}, \quad \mathbf{q} = \mu_{bx} \frac{d\mathbf{R}_0}{dt}, \quad \mu_{bx}^{-1} = M_b^{-1} + M_x^{-1}, \quad (11)$$

which corresponds to the relative momentum  $\mathbf{q}$ , is quite large. Even in the ground state of the molecule  $BX$ , this energy is on the order of its vibrational quantum  $\omega_0 \approx 0.3\text{--}0.5$  eV [24] due to the zero-point vibrations. Therefore, the previous above-mentioned scheme of  $\lambda(\varepsilon)$  transformation between CMS and LAB is not valid in general. In order to improve this scheme, it is indispensable to consider the  $a\mu$  atom collision with a real  $BX$  molecule of finite dimensions, instead of a point-like molecule  $BX$  that is located at the position of a free nucleus  $b$ .

The following relations between different vectors of the  $a\mu + BX$  system are inferred from Fig. 1:

$$\begin{aligned} \mathbf{R}_0 &= \mathbf{R}_x - \mathbf{R}_b = \mathbf{r}_x - \mathbf{r}_b, \\ \mathbf{R}_m &= \frac{M_b \mathbf{R}_b + M_x \mathbf{R}_x}{M_{bx}}, & \mathbf{r}_m &= \frac{M_b \mathbf{r}_b + M_x \mathbf{r}_x}{M_{bx}}, \\ \mathbf{R}_b &= \mathbf{R}_m - \frac{M_x}{M_{bx}} \mathbf{R}_0, & \mathbf{r}_b &= \mathbf{r}_m - \frac{M_x}{M_{bx}} \mathbf{R}_0, \\ \mathbf{R}_x &= \mathbf{R}_m + \frac{M_b}{M_{bx}} \mathbf{R}_0, & \mathbf{r}_x &= \mathbf{r}_m + \frac{M_b}{M_{bx}} \mathbf{R}_0, \end{aligned} \quad (12)$$

in which vectors  $\mathbf{R}_b$ ,  $\mathbf{R}_x$ , and  $\mathbf{R}_m$  denote the positions of the nuclei  $b$  and  $x$ , and their center of mass in LAB, respectively. Vectors  $\mathbf{r}_b$ ,  $\mathbf{r}_x$  and  $\mathbf{r}_m$  correspond to the relative positions of the particles.

The momentum  $\mathbf{p}$  of  $a\mu$  atom and the momentum  $\mathbf{p}_b$  of nucleus  $b$  in LAB are connected with the relative momentum  $\mathbf{k}$  [see Eq. (3)] by the following formulas [24]:

$$\mathbf{p} = -\mathbf{k} + \frac{M_{a\mu}}{M} \mathbf{P}, \quad (13)$$

$$\mathbf{p}_b = \mathbf{k} + \frac{M_b}{M} \mathbf{P}, \quad (14)$$

where  $M = M_a + M_b + M_\mu$  and  $\mathbf{P} = \mathbf{p} + \mathbf{p}_b$  are the total mass and momentum of the 3-body system ( $ab\mu$ ), respectively. The inverse relation for the momentum  $\mathbf{k}$  is evident from Eqs. (13)–(14):

$$\mathbf{k} = (M_{a\mu} \mathbf{p}_b - M_b \mathbf{p}) / M. \quad (15)$$

Analogously to Eqs. (13)–(14), the following relations

$$\mathbf{p}_b = -\mathbf{q} + \frac{M_b}{M_{bx}} \mathbf{P}_m, \quad (16)$$

$$\mathbf{p}_x = \mathbf{q} + \frac{M_x}{M_{bx}} \mathbf{P}_m, \quad (17)$$

$$\mathbf{P}_m = \mathbf{p}_x + \mathbf{p}_b, \quad (18)$$

hold for the LAB momenta  $\mathbf{p}_b$  and  $\mathbf{p}_x$  of the respective nuclei  $b$  and  $x$ , and the vector  $\mathbf{P}_m$  of the total momentum of molecule  $BX$ . The relative momentum  $\mathbf{q}$  of the nuclei  $b$  and  $x$  [see Eq. (11) and Fig. 1] is given by the expression

$$\mathbf{q} = (M_b \mathbf{p}_x - M_x \mathbf{p}_b) / M_{bx}, \quad (19)$$

which is similar to Eq. (15). By virtue of Eq. (16), the momentum (15) takes the following form:

$$\mathbf{k} = \frac{1}{M} \left( \frac{M_{a\mu} M_b}{M_{bx}} \mathbf{P}_m - M_{a\mu} \mathbf{q} - M_b \mathbf{p} \right). \quad (20)$$

From Fig. 1, one can infer the relation

$$\mathbf{r}_b = \mathbf{r}_m - \beta_b \mathbf{R}_0, \quad (21)$$

where  $\beta_b \mathbf{R}_0$  denotes the position of the molecule  $BX$  center of mass with respect to nucleus  $b$ :

$$\beta_b = \frac{M_x}{M_b + M_x} = \frac{\mu_{bx}}{M_b}. \quad (22)$$

The equation (21), together with the definitions (3), (9) and (11), leads to the following relation

$$\mathbf{k} = \mu \left( \frac{\mathbf{Q}}{\mu_t} - \beta_b \frac{\mathbf{q}}{\mu_{bx}} \right) \quad (23)$$

between the momenta  $\mathbf{k}$ ,  $\mathbf{q}$  and  $\mathbf{Q}$ . Analogously to Eq. (3), the relative kinetic energy  $\varepsilon$  can be expressed as

$$\varepsilon \equiv \varepsilon(\mathbf{Q}, \mathbf{q}) = \frac{\mu}{2} \left( \frac{\mathbf{Q}}{\mu_t} - \beta_b \frac{\mathbf{q}}{\mu_{bx}} \right)^2. \quad (24)$$

A relation between the formation rate  $\lambda(\varepsilon)$  in the center of mass of the  $a\mu + b$  system and the respective rate  $\lambda(E)$  in the LAB frame of the  $a\mu + BX$  system, which takes into account the internal motion of nucleus  $b$  within  $BX$ , can be written down in the form

$$\lambda(E, T) \equiv \lambda(\mathbf{p}, T) = \int \lambda(\varepsilon) dW(\mathbf{p}_b, \mathbf{p}_x) dF_T(\mathbf{P}), \quad (25)$$

where  $F_T(\mathbf{P}) \equiv F(\mathbf{P}, T)$  is the Maxwellian distribution of the molecules  $BX$  over their momenta  $\mathbf{P}$  in LAB

$$\begin{aligned} dF_T(\mathbf{P}) &= F(\mathbf{P}, T) d^3P \\ &= (2\pi M_{bx} T)^{-3/2} \exp(-\mathbf{P}^2/2M_{bx} T) d^3P, \end{aligned} \quad (26)$$

and  $W(\mathbf{p}_b, \mathbf{p}_x)$  is the distribution of nuclei  $b$  and  $x$

$$dW(\mathbf{p}_b, \mathbf{p}_x) = |\Psi(\mathbf{p}_b, \mathbf{p}_x)|^2 \frac{d^3 p_b}{(2\pi)^3} \frac{d^3 p_x}{(2\pi)^3} \quad (27)$$

with respect to the momenta  $\mathbf{p}_b$  and  $\mathbf{p}_x$  in the LAB frame. Function  $\Psi(\mathbf{p}_b, \mathbf{p}_x)$  denotes here the wave function of molecule  $BX$  in the momentum representation, which is equivalent to the real-space function

$$\Psi(\mathbf{r}_b, \mathbf{r}_x) = \exp(i\mathbf{P} \cdot \mathbf{R}_m) \Phi(\mathbf{R}_0), \quad (28)$$

with both the total momentum  $\mathbf{P}$  and the center-of-mass position  $\mathbf{R}_m$  of  $BX$  given in LAB. In the momentum representation, the function (28) has the following form:

$$\begin{aligned} \Psi(\mathbf{p}_b, \mathbf{p}_x) &= \int \Psi(\mathbf{r}_b, \mathbf{r}_x) \exp(-i\mathbf{p}_b \cdot \mathbf{r}_b) \\ &\quad \exp(-i\mathbf{p}_x \cdot \mathbf{r}_x) d^3 r_b d^3 r_x. \end{aligned} \quad (29)$$

Upon employing the expression

$$\mathbf{p}_b \cdot \mathbf{r}_b + \mathbf{p}_x \cdot \mathbf{r}_x = \mathbf{q} \cdot \mathbf{R}_0 + \mathbf{P}_m \cdot \mathbf{R}_m, \quad (30)$$

which follows from Eqs. (12)–(14), and changing the variables  $d^3r_b d^3r_x \rightarrow d^3R_m d^3R_0$  in Eq. (29), we obtain

$$\begin{aligned} \Psi(\mathbf{p}_b, \mathbf{p}_x) &= \int \Phi(\mathbf{R}_0) \exp(-i\mathbf{q} \cdot \mathbf{R}_0) \\ &\quad \exp[-i(\mathbf{P}_m - \mathbf{P}) \cdot \mathbf{R}_m] d^3R_0 d^3R_m. \end{aligned} \quad (31)$$

Then, using the following representation of the Dirac delta function

$$\int \exp[-i(\mathbf{P}_m - \mathbf{P}) \cdot \mathbf{R}_m] d^3R_m = (2\pi)^3 \delta(\mathbf{P}_m - \mathbf{P}) \quad (32)$$

and the definition

$$\psi(\mathbf{q}) \equiv \int \Phi(\mathbf{R}_0) \exp(-i\mathbf{q} \cdot \mathbf{R}_0) d^3R_0, \quad (33)$$

equation (31) leads to the relation

$$|\Psi(\mathbf{p}_b, \mathbf{p}_x)|^2 = [(2\pi)^3 \delta(\mathbf{P}_m - \mathbf{P})]^2 |\psi(\mathbf{q})|^2. \quad (34)$$

This relation can be simplified on employing the following formula [25]:

$$\delta(x - a)\delta(x - b) = V\delta(x - a), \quad (35)$$

in which the arbitrary constant corresponds to the normalization of volume:  $V = 1$ . Then, the expression (34) can be written as

$$|\Psi(\mathbf{p}_b, \mathbf{p}_x)|^2 = (2\pi)^3 \delta(\mathbf{P}_m - \mathbf{P}) |\psi(\mathbf{q})|^2. \quad (36)$$

The formation rate (25) in LAB now takes the form

$$\lambda(\mathbf{p}, T) = \int \lambda(\varepsilon) F(\mathbf{P}, T) d^3P |\psi(\mathbf{q})|^2 \frac{d^3q}{(2\pi)^3}, \quad (37)$$

by virtue of Eqs. (26), (27), (36), and the subsequent change  $d^3p_b d^3p_x \rightarrow d^3P_m d^3q$ , of the integration variables and the integration over  $d^3P_m$ .

Using Eqs. (18) and (19) the collision energy  $\varepsilon$  defined in Eq. (3) can be expressed in terms of the LAB momenta

$$\varepsilon = \frac{1}{2\mu M^2} \left( M_b \mathbf{P} + M_{a\mu} \mathbf{q} - \frac{M_{a\mu} M_b}{M_{bx}} \mathbf{P} \right)^2. \quad (38)$$

Now, the rate (37) can be written down as follows [22]:

$$\lambda(E, T) \equiv \lambda(\mathbf{p}, T) = \int F(\mathbf{P}, T) \Lambda(\varepsilon_Q) d^3P, \quad (39)$$

where

$$\begin{aligned}\Lambda(\varepsilon_Q) &\equiv \int |\psi(\mathbf{q})|^2 \frac{d^3q}{(2\pi)^3} \int_0^\infty \delta(\varepsilon - \tilde{\varepsilon}) \lambda(\tilde{\varepsilon}) d\tilde{\varepsilon} \\ &= \int_0^\infty \lambda(\tilde{\varepsilon}) g(\varepsilon_Q, \tilde{\varepsilon}) d\tilde{\varepsilon},\end{aligned}\tag{40}$$

and the notation

$$g(\varepsilon_Q, \tilde{\varepsilon}) \equiv \int |\psi(\mathbf{q})|^2 \delta(\varepsilon - \tilde{\varepsilon}) \frac{d^3q}{(2\pi)^3}\tag{41}$$

is introduced. The characteristic quantity  $\Lambda(\varepsilon_Q)$  in Eq. (39) can be considered as the “formation rate” in the *molecular* CMS, which has been obtained upon the rate transformation from the *nuclear* CMS and then averaged over the momenta  $\mathbf{q}$  of the nuclei with the distribution function  $g(\varepsilon_Q, \tilde{\varepsilon})$ , in accordance with Eqs. (38) and (11). Finally, Eq. (39) for the formation rate in LAB is reduced to the form similar to that of formula (5):

$$\begin{aligned}\lambda(\mathbf{p}, T) &= \int F(\mathbf{P}, T) d^3P \int_0^\infty \delta(\varepsilon_Q - \tilde{\varepsilon}_Q) \Lambda(\tilde{\varepsilon}_Q) d\tilde{\varepsilon}_Q \\ &= \int_0^\infty \Lambda(\tilde{\varepsilon}_Q) G(\mathbf{p}, \tilde{\varepsilon}_Q) d\tilde{\varepsilon}_Q,\end{aligned}\tag{42}$$

where the “distribution” function  $G(\mathbf{p}, \varepsilon_Q)$  is defined as

$$G(\mathbf{p}, \varepsilon_Q) \equiv \int \delta(\varepsilon_Q - \tilde{\varepsilon}_Q) F(\mathbf{P}, T) d^3P.\tag{43}$$

According to Ref. [22], the function (43) is identical with that defined by Eq. (6). Using the definitions (7)–(9), the latter function can also be written down in the following form:

$$\begin{aligned}G(E, \varepsilon_Q) &= \sqrt{\frac{M_t}{\pi\mu_t T}} \frac{1}{\sqrt{E}} \exp\left[-\frac{M_{bx}}{T} \left(\frac{\varepsilon_Q}{\mu_t} + \frac{E}{M_{a\mu}}\right)\right] \\ &\quad \sinh\left(\frac{2M_{bx}}{T} \sqrt{\frac{\varepsilon_Q E}{\mu_t M_{a\mu}}}\right).\end{aligned}\tag{44}$$

In particular, for  $E \rightarrow 0$ , one has:

$$G(E, \varepsilon_Q) = 2\sqrt{\frac{1}{\pi T^3} \left(\frac{M_{bx}}{\mu_t}\right)^3} \sqrt{\varepsilon_Q} \exp\left(-\frac{M_{bx}}{\mu_t} \frac{\varepsilon_Q}{T}\right).\tag{45}$$

### III. INTERNAL NUCLEAR MOTION WITHIN A HYDROGENIC MOLECULE

Equation (24) can be expressed [see definitions (9) and (11)] in terms of kinetic energies  $\varepsilon_Q$  and  $\varepsilon_q$ , which correspond to the momenta  $\mathbf{Q}$  and  $\mathbf{q}$ , respectively:

$$\begin{aligned}\varepsilon &= \mu \left( \frac{\varepsilon_Q}{\mu_t} + \beta_b^2 \frac{\varepsilon_q}{\mu_{bx}} - 2\beta_b \sqrt{\frac{\varepsilon_Q \varepsilon_q}{\mu_t \mu_{bx}}} z \right), \\ z &= \cos \vartheta,\end{aligned}\tag{46}$$



where the angle between vectors  $\mathbf{Q}$  and  $\mathbf{q}$  is denoted by  $\vartheta$ . When  $\varepsilon_Q \gg \varepsilon_q$ , equation (46) takes a simple asymptotic form (10):  $\varepsilon = (\mu/\mu_t)\varepsilon_Q$ . On the other hand, when  $\varepsilon_Q \ll \varepsilon_q$ , kinetic energy  $\varepsilon$  is mainly determined by the internal molecular energy  $\varepsilon_q$ . In particular, at  $\varepsilon_Q \rightarrow 0$ , the characteristic energy  $\varepsilon$  tends to a constant value, which is given by the second term of Eq. (46). The width of  $\varepsilon$  spectrum is ruled by the term  $\sqrt{\varepsilon_Q \varepsilon_q}$  and thus rises with increasing  $\varepsilon_Q$ . On the other hand, as Eq. (46) indicates, a fixed kinetic energy  $\varepsilon_Q$  (9) in CM of the *molecular*  $a\mu + BX$  system corresponds to a wide spectrum of energies  $\varepsilon$  in the *nuclear* CMS. As a result, the formation rate  $\Lambda(\varepsilon_Q)$  in the *molecular* CMS, which is given in Eq. (40), has been obtained on averaging the *input* formation rates  $\lambda(\varepsilon)$  over such a spectrum. This leads to an additional smearing of these rates (apart from the thermal motion of the molecules), if they significantly change within the spectrum of energies  $\varepsilon$ . This problem has already been considered in the case of  $a\mu$  scattering from hydrogenic molecules [26], where it has been shown there that the above-mentioned smearing effect is of importance for many low-energy scattering cross sections  $a\mu + BX$ .

In order to obtain the distribution  $g(\varepsilon_Q, \varepsilon)$  as a function of collision energies  $\varepsilon$  in the *nuclear* CMS for a fixed collision energy  $\varepsilon_Q$  in the *molecular* CMS [see Eq. (46)], we follow the calculating scheme from Ref. [26]. It is assumed here that the orientation of molecule with respect to the vector  $\mathbf{r}_m$  is random. In a general case, the wave function  $\Phi_n(\mathbf{R}_0)$  of molecule  $BC$  in the quantum state  $n$  can be written as follows:

$$\Phi_n(\mathbf{R}_0) = \frac{u_\nu(R_0)}{R_0} Y_{KM_K}(\hat{\mathbf{R}}_0), \quad \hat{\mathbf{R}}_0 \equiv \frac{\mathbf{R}_0}{R_0}, \quad (47)$$

where  $n \equiv (\nu, K, M_K)$ , the vibrational quantum number is denoted by  $\nu$ , the rotational state is specified by the quantum numbers  $K$  and  $M_K$ , and  $Y_{KM_K}$  stands for the corresponding spherical harmonics. The radial wave function  $u_\nu$  in the harmonic approximation takes the form

$$u_\nu(R_0) = \mathcal{N}_\nu H_\nu(\alpha \rho_0) \exp\left(-\frac{1}{2}\alpha^2 \rho_0^2\right), \quad (48)$$

$$\mathcal{N}_\nu = \sqrt{\frac{\alpha}{2^\nu \nu! \sqrt{\pi}}}, \quad \alpha = \sqrt{\mu_{bx} \omega_0}, \quad \rho_0 = R_0 - \bar{R}_0,$$

where  $H_\nu$  denotes the  $\nu$ -th Hermite polynomial and  $\rho_0$  is the displacement of  $R_0$  from a mean distance  $\bar{R}_0$  between the nuclei  $b$  and  $x$  in  $BX$ . The rotational  $E_K$  and vibrational  $E_\nu$  energy levels are given as

$$E_K = B_{\text{rot}} K(K+1), \quad E_\nu = \left(\nu + \frac{1}{2}\right) \omega_0, \quad (49)$$

where the rotational  $B_{\text{rot}}$  and vibrational  $\omega_0$  constants depend on the type of hydrogen isotopes  $b$  and  $x$ .

At temperatures usually applied in experiments, the molecules are in the ground vibrational state  $\nu = 0$ . Thus, the probability density (41) for this state ( $n = 0 \equiv (\nu = 0, K, M_K)$ ) takes the form

$$g(\varepsilon_Q, \tilde{\varepsilon}) = \int \left| \int \exp(-i\mathbf{q} \cdot \mathbf{R}_0) \Phi_0(\mathbf{R}_0) d^3 R_0 \right|^2 \delta(\varepsilon - \tilde{\varepsilon}) \frac{d^3 q}{(2\pi)^3}, \quad (50)$$

The substitution of the functions (47)–(48) into Eq. (50) results in

$$g(\varepsilon_Q, \tilde{\varepsilon}) = \int f_{0K}(q) |Y_{KM_K}(\hat{\mathbf{q}})|^2 \delta(\varepsilon - \tilde{\varepsilon}) d^3q, \quad (51)$$

where

$$f_{0K}(q) \equiv \frac{2\alpha}{\sqrt{\pi^3}} \mathcal{J}_R^2(q; K), \quad \hat{\mathbf{q}} = \mathbf{q}/q, \quad (52)$$

$$\mathcal{J}_R(q; K) = \int_0^\infty j_K(qR_0) \exp\left(-\frac{1}{2}\alpha^2 \rho_0^2\right) R_0 dR_0, \quad (53)$$

and  $j_K(qR_0)$  denotes the  $K$ -th spherical Bessel function. The main contribution to the integral (53) comes from the vicinity of  $\rho_0 \approx 0$  ( $R_0 \approx \bar{R}_0$ ). Thus, we obtain a good approximation of  $\mathcal{J}_R$  if the lower integration limit is extended to  $-\infty$ . Then, we can use the asymptotic form of the function  $j_K(x)$  for  $x \gg K(K+1)$  [27]

$$j_K(x) \approx \frac{1}{x} \cos\left[x - \frac{1}{2}(K+1)\pi\right], \quad (54)$$

which is the exact form for  $K = 0$  at any  $x$ . As a result, we obtain the following approximation:

$$\mathcal{J}_R(q; K) \approx \sqrt{2\pi} \frac{\bar{R}_0}{\alpha} j_K(q\bar{R}_0) \exp\left(-\frac{q^2}{2\alpha^2}\right). \quad (55)$$

In the case of  $K > 0$  and  $q\bar{R}_0 \lesssim K(K+1)$ , the integral  $\mathcal{J}_R$  should be estimated numerically.

Further evaluation of Eq. (51) for  $g(\varepsilon_Q, \tilde{\varepsilon}) \equiv g_K(\varepsilon_Q, \tilde{\varepsilon})$  is performed using the additional averaging over the projections  $M_K$  with a uniform weight  $(2K+1)^{-1}$  for a fixed  $K$

$$\begin{aligned} g_K(\varepsilon_Q, \tilde{\varepsilon}) &= \frac{1}{2K+1} \sum_{M_K} \int f_{0K}(q) |Y_{KM_K}(\hat{\mathbf{q}})|^2 \delta(\varepsilon - \tilde{\varepsilon}) d^3q \\ &= \int_0^\infty f_{0K}(q) q^2 dq \int_0^{2\pi} \frac{1}{2K+1} \sum_{M_K} \mathcal{J}_{KM_K}(\varepsilon_q) d\phi. \end{aligned} \quad (56)$$

Here, the integral  $\mathcal{J}_{KM_K}(\varepsilon_q)$  is specified as

$$\mathcal{J}_{KM_K}(\varepsilon_q) = \int_0^\pi |Y_{KM_K}(\vartheta, \phi)|^2 \delta(\varepsilon - \tilde{\varepsilon}) \sin \vartheta d\vartheta \quad (57)$$

and the solid angle  $\Omega(\vartheta, \phi)$  determines the orientation of vector  $\mathbf{q}$  with respect to a fixed vector  $\mathbf{Q}$ :  $d\Omega = \sin \vartheta d\vartheta d\phi = dz d\phi$ . Then, on using the relation (46), Eq. (57) can be expressed as the following integral

$$\begin{aligned} \mathcal{J}_{KM_K} &= \int_{-1}^1 |Y_{KM_K}(\vartheta, \phi)|^2 \delta\left(\frac{\mu}{\mu_t} \varepsilon_Q + \beta_b^2 \frac{\mu}{\mu_{bx}} \varepsilon_q \right. \\ &\quad \left. - \tilde{\varepsilon} - 2\beta_b \frac{\mu}{\sqrt{\mu_t \mu_{bx}}} \sqrt{\varepsilon_Q \varepsilon_q} z\right) dz \end{aligned} \quad (58)$$

with respect to the variable  $z$ . The delta function impose the following condition on  $z$ :

$$z = z_0 \equiv \cos \vartheta_0, \quad z_0 = \frac{1}{2\beta_b} \frac{\sqrt{\mu_t \mu_{bx}}}{\mu} \frac{1}{\sqrt{\varepsilon_Q \varepsilon_q}} \left( \frac{\mu}{\mu_t} \varepsilon_Q + \beta_b^2 \frac{\mu}{\mu_{bx}} \varepsilon_q - \tilde{\varepsilon} \right), \quad (59)$$

for all  $z_0$  such that  $|z_0| \leq 1$ . The result of the integration over  $z$  can be written down as

$$\mathcal{J}_{KM_K} = \frac{1}{2\beta_b} \frac{\sqrt{\mu_t \mu_{bx}}}{\mu} \frac{1}{\sqrt{\varepsilon_Q \varepsilon_q}} \Theta(\varepsilon_q - \varepsilon_{Q_1}) \Theta(\varepsilon_{Q_2} - \varepsilon_q) |Y_{KM_K}(\vartheta_0, \phi)|^2, \quad (60)$$

where  $\Theta$  is the Heaviside step function and

$$\varepsilon_{Q_{1,2}} = \frac{1}{\beta_b^2} \frac{\mu_{bx}}{\mu \mu_t} \left( \sqrt{\mu_t} \tilde{\varepsilon} \mp \sqrt{\mu \varepsilon_Q} \right)^2. \quad (61)$$

Substituting Eq. (60) into Eq. (56) and changing the integration variable  $q$  to variable  $\varepsilon_q$ , which is defined in Eq. (11), lead to the following relation

$$g_K(\varepsilon_Q, \tilde{\varepsilon}) = \frac{1}{2\beta_b} \frac{\sqrt{\mu_t \mu_{bx}}}{\mu} \frac{1}{\sqrt{\varepsilon_Q}} \int_{\varepsilon_{Q_1}}^{\varepsilon_{Q_2}} f_{0K}(\varepsilon_q) d\varepsilon_q \int_0^{2\pi} \frac{1}{2K+1} \sum_{M_K} |Y_{KM_K}(\vartheta_0, \phi)|^2 d\phi, \quad (62)$$

where

$$f_{0K}(\varepsilon_q) \equiv \sqrt{2\mu_{bx}^3} f_{0K}(q(\varepsilon_q)). \quad (63)$$

The integration over  $\phi$  in Eq. (62) gives the factor of  $1/2$ , since for any  $\Omega$  one has

$$\frac{1}{2K+1} \sum_{M_K} |Y_{KM_K}(\Omega)|^2 = \frac{1}{4\pi}. \quad (64)$$

Thus, for a random-oriented molecule,

$$g_K(\varepsilon_Q, \tilde{\varepsilon}) = \frac{1}{4\beta_b} \frac{\sqrt{\mu_t \mu_{bx}}}{\mu} \frac{1}{\sqrt{\varepsilon_Q}} \int_{\varepsilon_{Q_1}}^{\varepsilon_{Q_2}} f_{0K}(\varepsilon_q) d\varepsilon_q. \quad (65)$$

Employing a convenient variable

$$\omega = 2\varepsilon_q/\omega_0 \quad (66)$$

and Eqs. (11), (48) and (63), the distribution (65) takes the final form

$$g_K(\varepsilon_Q, \tilde{\varepsilon}) = \frac{\alpha^4}{\beta_b \sqrt{(2\pi)^3}} \frac{\sqrt{\mu_t \mu_{bx}}}{\mu} \frac{1}{\sqrt{\omega_0 \varepsilon_Q}} \int_{\omega_1}^{\omega_2} \mathcal{J}_R^2(\alpha\sqrt{\omega}; K) d\omega, \quad \omega_{1,2} \equiv \frac{2\varepsilon_{Q_{1,2}}}{\omega_0}, \quad (67)$$

for a fixed collision energy  $\varepsilon_Q$  in the *molecular* CMS.

Let us consider the limit  $\varepsilon_Q \rightarrow 0$ . Then, according to Eq. (46), the corresponding distribution of  $\tilde{\varepsilon}$  is solely determined by the distribution of internal kinetic energy  $\varepsilon_q$  of the molecule  $BX$ :

$$\tilde{\varepsilon} \sim \varepsilon_q \gg \varepsilon_Q. \quad (68)$$

In this approximation

$$\begin{aligned} \omega_{1,2} &\approx \tilde{\omega} = \frac{2}{\beta_b^2} \frac{\mu_{bx}}{\mu} \frac{\tilde{\varepsilon}}{\omega_0}, \\ d\omega &\rightarrow \Delta\omega = \omega_2 - \omega_1 = \frac{8}{\beta_b^2} \frac{\mu_{bx}}{\sqrt{\mu_t \mu}} \frac{\sqrt{\varepsilon_Q \tilde{\varepsilon}}}{\omega_0}, \end{aligned} \quad (69)$$

so that

$$g_K(\varepsilon_Q, \tilde{\varepsilon}) = \frac{2\alpha^4}{\beta_b^2 \sqrt{\pi^3}} \frac{\mu_{bx}}{\mu} \frac{1}{\omega_0} \sqrt{\tilde{\omega}} \mathcal{J}_R^2(\alpha \sqrt{\tilde{\omega}}; K), \quad (70)$$

when  $\varepsilon_Q \rightarrow 0$ . In this limit, if the approximation (55) is valid, Eqs. (67) and (70) take the following asymptotic forms:

$$\begin{aligned} g_K(\varepsilon_Q, \tilde{\varepsilon}) &= \frac{\alpha^2 \bar{R}_0^2}{\beta_b \sqrt{2\pi}} \frac{\sqrt{\mu_t \mu_{bx}}}{\mu} \frac{1}{\sqrt{\omega_0 \varepsilon_Q}} \\ &\quad \int_{\omega_1}^{\omega_2} j_K^2(\alpha \bar{R}_0 \sqrt{\omega}) \exp(-\omega) d\omega \end{aligned} \quad (71)$$

and

$$g_K(\varepsilon_Q, \tilde{\varepsilon}) = \frac{4\alpha^2 \bar{R}_0^2}{\beta_b^2 \sqrt{\pi}} \frac{\mu_{bx}}{\mu} \frac{1}{\omega_0} \sqrt{\tilde{\omega}} j_K^2(\alpha \bar{R}_0 \sqrt{\tilde{\omega}}) \exp(-\tilde{\omega}), \quad (72)$$

respectively.

In the limit  $\varepsilon_Q \rightarrow \infty$ , the argument of the  $\delta$  function in Eq. (58) tends to  $\tilde{\varepsilon} - \mu \varepsilon_Q / \mu_t$ , which means that

$$\tilde{\varepsilon} \rightarrow \frac{\mu}{\mu_t} \varepsilon_Q, \quad \text{when } \varepsilon_Q \rightarrow \infty. \quad (73)$$

Let us note once more that it is invalid to use the above asymptotic relation, which is equivalent to Eq. (10), when the condition  $\varepsilon_Q \gg \varepsilon_q \sim \omega_0/4$  is not fulfilled.

#### IV. RESULTS AND DISCUSSION

The distribution density (67), which was calculated using a numerical integration in the case of  $p\mu + \text{H}_2$  system, is shown<sup>2</sup> in Fig. 2 as a function of kinetic energy  $\varepsilon$  in the *nuclear* CMS for several values of  $\varepsilon_Q$  (in the *molecular* CMS). Since the characteristic kinetic energy  $\omega_{bx}$  in the molecular ground state is determined by the zero-point vibrations:  $\omega_{bx} \sim \frac{1}{2} E_{\nu=0} = \omega_0/4$ , the magnitude of  $\omega_{bx}$  for the  $\text{H}_2$  molecule is on the order of 0.1 eV. Therefore, the curve plotted in Fig. 2 for  $\varepsilon_Q = 0.001$  eV practically represents the limit (70). It is evident that the averaging over the distribution density  $g \equiv g_K$  in Eq. (40) is important when the rate

---

<sup>2</sup> For a simplicity of the notation, the integration variable  $\tilde{\varepsilon}$  in the presented plots of the functions (67) and (70) is displayed without the “tilde” sign.

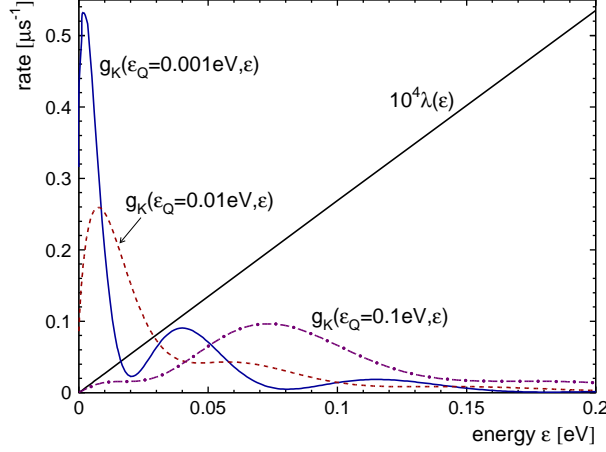


FIG. 2. (Color online) Function  $g_{K=0}(\varepsilon_Q, \varepsilon)$  for  $p\mu + \text{H}_2$  at  $\varepsilon_Q = 0.001, 0.01$ , and  $0.1$  eV (in arbitrary units), together with the rate  $\lambda(\varepsilon)$  of nonresonant  $pp\mu$  formation in the transition  $J = 1 \rightarrow J = 1, v = 0$ .

$\lambda(\varepsilon)$  significantly changes within the characteristic width of  $g_K$ , which occurs in the case of  $pp\mu$  formation presented in this figure.

The dependence of  $g_K$  on the rotational quantum numbers  $K$  is shown in Figs. 3 and 4 for  $\varepsilon_Q = 0.001$  and  $1$  eV, respectively. At  $\varepsilon_Q \lesssim 0.001$  eV, the distribution of  $\varepsilon$  is practically determined by the rotational-vibrational state of the  $\text{H}_2$  molecule. However, this distribution

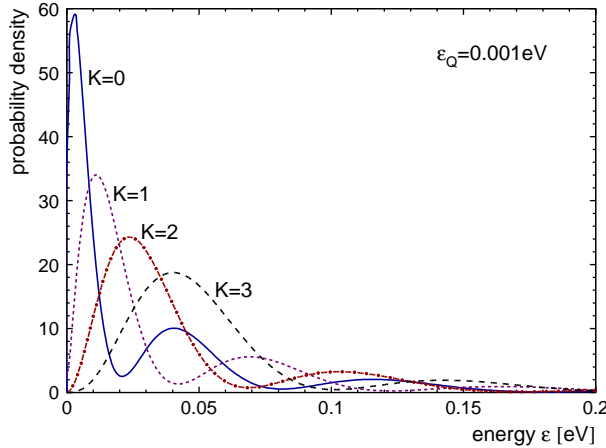


FIG. 3. (Color online) The distribution density  $g_K(\varepsilon_Q = 0.001 \text{ eV}, \varepsilon; K)$  for various rotational quantum numbers  $K$  in the case of  $p\mu + \text{H}_2$  process.

strongly changes for subsequent rotational numbers. The distribution maximum decreases with rising  $K$ . At  $\varepsilon_Q \gtrsim 1$  eV, the location of maximum of  $g_K$  is proportional to  $\varepsilon_Q$ , according to the asymptotic relation (73). The rotational-vibrational motion of the molecule causes a significant broadening of this maximum, which is wider at higher  $\varepsilon_Q$ . The distribution  $g_K$  is flatter for greater  $K$ . The presented changes of  $g_K$  for various  $K$  can lead to an appreciable dependence of the formation rates (39) and (40) on the initial rotational distribution of the target molecules.

In order to demonstrate effects of the internal nuclear motion in the target molecules,

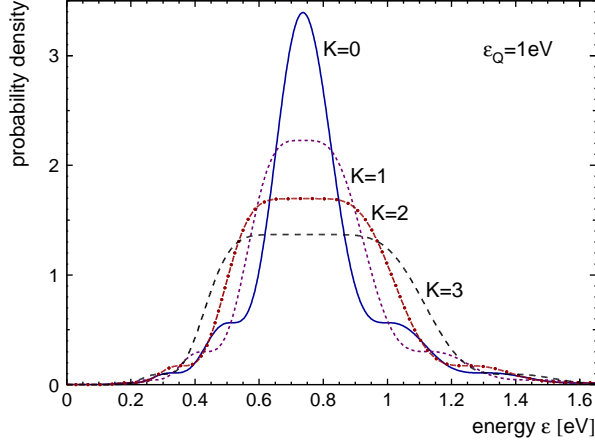


FIG. 4. (Color online) The same as in Fig. 3 for  $\varepsilon_Q = 1$  eV.

the *molecular* formation rate  $\Lambda(\varepsilon_Q(\varepsilon))$ , which was calculated using Eq. (40), and the input *nuclear* formation rate  $\lambda(\varepsilon)$  are plotted below for some interesting cases. For the sake of comparison, the pairs of the corresponding rates  $\Lambda(\varepsilon_Q(\varepsilon))$  and  $\lambda(\varepsilon)$  are shown together using the asymptotic relation (73) between kinetic energies  $\varepsilon_Q$  and  $\varepsilon$ . Since we consider target temperatures  $T \leq 300$  K, the hydrogenic molecules are always in the ground vibrational state  $\nu = 0$ .

The internal-motion effect in  $pp\mu$  formation for the transition  $J = 0 \rightarrow J = 0$ ,  $v = 0$  is shown in Fig. 5. The apparent difference between the rates below about 0.2 eV is due to

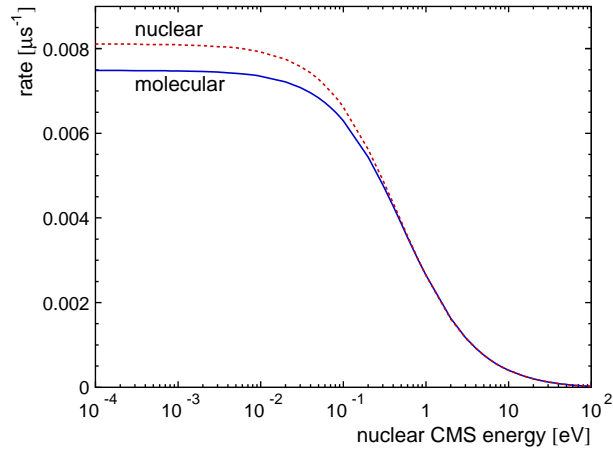


FIG. 5. (Color online) The rates  $\Lambda$  (*molecular*) and  $\lambda$  (*nuclear*) of nonresonant  $pp\mu$  formation versus kinetic energy  $\varepsilon$ , for the transition  $J = 0 \rightarrow J = 0$  in collision  $p\mu + \text{H}_2(K = 0)$ .

a significant variation of the input rate  $\lambda(\varepsilon)$  within a relatively narrow interval  $5 \text{ meV} \lesssim \varepsilon \lesssim 0.2 \text{ eV}$ , which is comparable with the characteristic width of the distribution  $g_K$ . This effect disappears at higher energies. The nuclear-motion smearing of the formation rate for the  $pp\mu$  formation in the transition  $J = 1 \rightarrow J = 0$  is shown in Fig. 6. Here, this effect is due to the small magnitude of  $\lambda(\varepsilon)$  for the  $p\mu + p$  scattering at  $\varepsilon \rightarrow 0$  in the initial  $J = 1$  state. In general, such a behavior is typical for the nonresonant formation at the muonic atom scattering in higher partial ( $J > 0$ ) wave state.

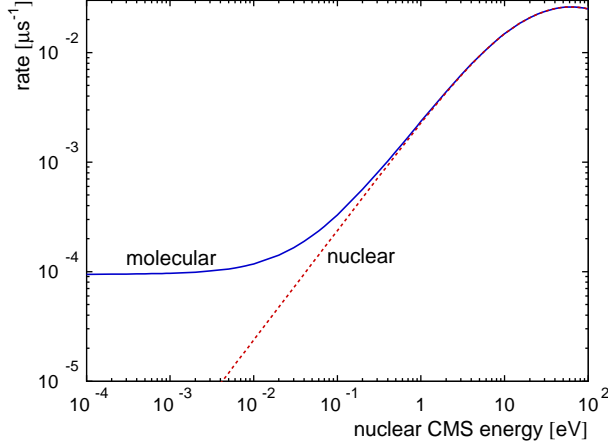


FIG. 6. (Color online) The same as in Fig. 5 for the transition  $J = 1 \rightarrow J = 0$ .

A dependence of the formation rate  $\Lambda$  on the initial rotational state of the target molecule is shown in Fig. 7, for the  $pp\mu$  formation in the transition  $J = 0 \rightarrow J = 0$ . The appre-

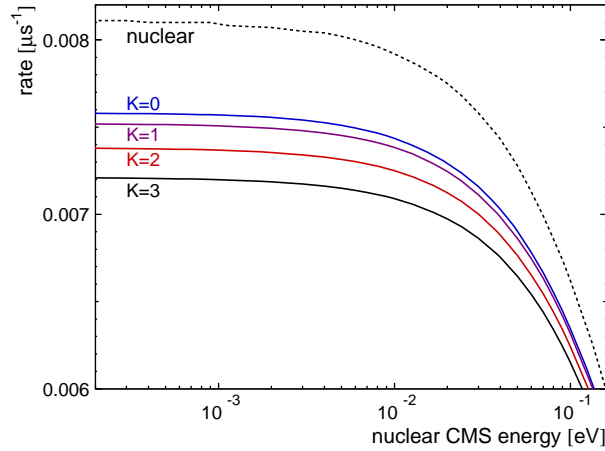


FIG. 7. (Color online) The same as in Fig. 5. The *molecular* rates  $\Lambda$  (solid lines) are calculated for the initial rotational states  $K = 0, 1, 2$ , and  $3$  of the  $H_2$  molecule.

ciable differences of  $\Lambda$  for various  $K$  lead to different values of the average formation rate  $\lambda(E, T)$  in the LAB frame, depending on the rotational population for a specified target and temperature. For example, strong nuclear-motion and rotational effects occur at relatively high energies (target temperatures) for the transition  $J = 2 \rightarrow J = 2$  in the nonresonant  $tt\mu$  formation within the  $T_2$  molecule (see Fig. 8). This is due to the existence of the  $tt\mu$  quasi-stationary state, which appears as a narrow peak in the elastic  $t\mu + t$  cross-section at the scattering energy  $\sim 3$  eV and  $J = 2$  [28, 29].

Figure 9 refers to the nonresonant formation of the  $dd\mu$  molecule (2) in the loosely-bound state  $J = v = 1$  (see details in Ref. [18]). For the thermalized  $d\mu$  atoms, the nonresonant process (2) is unfeasible. However, such a reaction is effective in the case of nonthermalized  $d\mu$  atoms with collision energies exceeding the ionization threshold of the  $D_2$  molecule. The rate  $\Lambda(\varepsilon_Q(\varepsilon))$  plotted in this figure was estimated by averaging the corresponding input rate  $\lambda(\varepsilon)$  for  $dd\mu$  formation in the  $J = v = 1$  state [18], with the use of Eqs. (40) and (67).

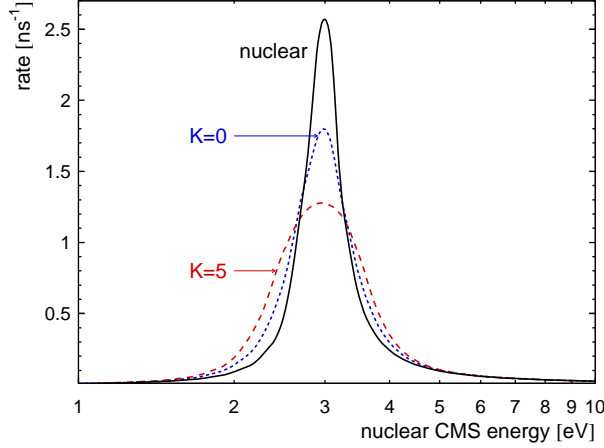


FIG. 8. (Color online) The *molecular*  $\Lambda$  (for  $K = 0$  and  $5$ , dashed lines) rates and the *nuclear*  $\lambda$  rate for the nonresonant  $tt\mu$  formation in the transition  $J = 2 \rightarrow J = 2$ .

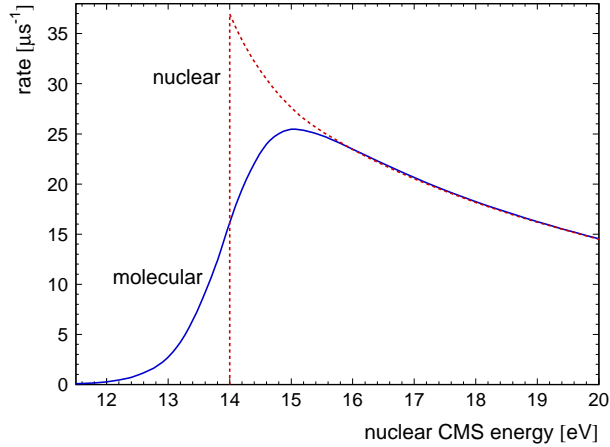


FIG. 9. (Color online) The total *molecular*  $\Lambda$  (solid line) and *nuclear*  $\lambda$  (dashed line) rates of nonresonant  $dd\mu$  formation in the  $J = v = 1$  state versus energy  $\varepsilon$ . The Boltzmann population of the rotational energy levels of  $D_2$  for  $T = 300$  K is assumed.

A smearing of the rate  $\Lambda$  due to the internal nuclear motion is quite strong near the threshold. However, this effect cannot significantly affect the kinetics of  $dd$ -fusion, since the threshold is located at energy much higher than the thermal energies of typical  $D_2$  targets. Thus, a fraction of the nonthermalized  $d\mu$  atoms with such high energies ( $\sim 15$  eV) is small. The analogous around-threshold smearing effect is shown in Fig. 10 for nonresonant formation of the  $dt\mu$  molecule in the loosely-bound state  $J = v = 1$ . This muonic molecule is created in the collision of  $t\mu$  with the  $D_2$  molecule. In this case, the threshold energy of 16 eV is somewhat greater than that for the  $dd\mu$  molecule.

The *molecular* rates  $\Lambda(E)$  of nonresonant  $dd\mu$  formation in the state  $J = 0$ , in the case of  $d\mu$  collision with the molecules  $D_2$  and  $HD$ , are presented in Fig. 11 as functions of LAB kinetic energy  $E$ . These rates were calculated using Eqs. (42) and (44). The corresponding *nuclear* rate  $\lambda(E)$  is plotted for a comparison. A strong smearing of  $\Lambda(E)$  appears at low collision energies ( $E \lesssim 0.1$  eV), where the input rate  $\lambda(\varepsilon)$  rises rapidly in the interval of



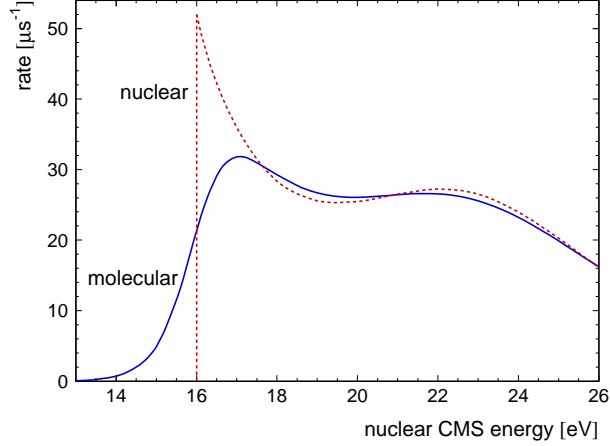


FIG. 10. (Color online) The same as in Fig. 9 for the  $dt\mu$  formation in the state  $J = v = 1$  in collision  $t\mu + D_2$ .

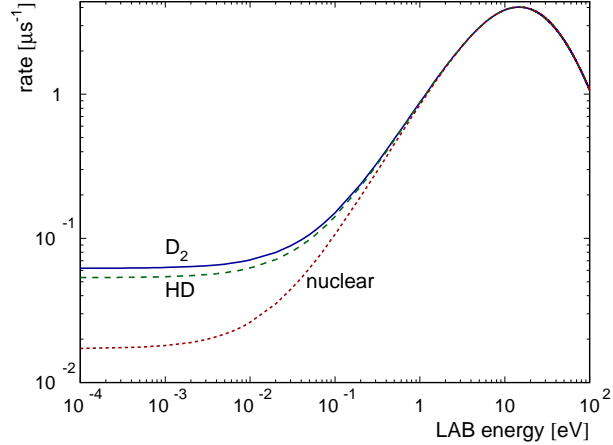


FIG. 11. (Color online) The rate  $\Lambda(E)$  of nonresonant  $dd\mu$  formation in the  $J = 0$  state in  $d\mu$  collision with the target molecules  $D_2$  and  $HD$  versus LAB energy  $E$ . The molecules have the Boltzmann populations of their rotational levels for 30 K.

energies  $\varepsilon \ll \omega_0$ . As a result, the molecular rates are much greater than the corresponding nuclear rate for thermalized  $d\mu$  atoms. Also, an appreciable isotopic effect can be observed in Fig. 11 at low energies. This effect is due to the different distributions  $g(\varepsilon_Q, \varepsilon)$  of the deuteron kinetic energy in the molecules  $D_2$  and  $HD$ . Since most kinetic energy in the  $HD$  molecule is carried by the lighter proton, it follows that the mean kinetic energy of deuteron in  $HD$  is smaller than that in the  $D_2$  molecule. Let us note that the nonresonant  $dd\mu$  formation rate in the state  $(J = 1, v = 0)$  is very flat at low collision energies. As a result, there is no appreciable differences between the rates  $\lambda(E)$  and  $\Lambda(E)$  in this case.

Significant differences between the rates  $\lambda(E)$  and  $\Lambda(E)$  at lowest energies are of special importance when the conditions of steady-state kinetics are reached, e.g., as in the case of experiments reported in Ref. [3]. Under such conditions, the kinetics is described in terms of the thermally averaged rates of various  $\mu CF$  processes for a fixed target temperature. In calculations it is assumed that the distributions of LAB kinetic energies of the molecules and

muonic atoms in a gaseous target have the Maxwellian shape. The rotational levels of the target molecules obey the Boltzmann distribution. The thermally-averaged total nonresonant rates  $\lambda(T)$  and  $\Lambda(T)$  are plotted in Fig. 12 as functions of the target temperature, for

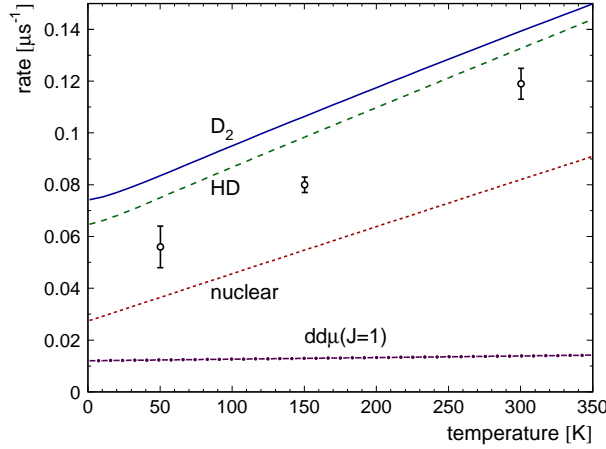


FIG. 12. (Color online) The thermally averaged total rates  $\lambda(T)$  and  $\Lambda(T)$  (for  $D_2$  and HD) of nonresonant  $dd\mu$  formation as functions of the target temperature  $T$ . The experimental data for the HD target are taken from Ref. [3]. A contribution from the  $J = 1$  state is also plotted (dash-dotted line).

the  $D_2$  and HD gases. Also, the contribution from the state  $J = 1$  to the total rate is shown, which is practically identical for both the nuclear and molecular rates. The experimental data points at  $T = 50, 150$ , and  $300$  K were determined in Ref. [3] using the steady-state kinetics for a pure HD target. The calculated rates  $\lambda(T)$  and  $\Lambda(T)$  do not well describe the data. Nevertheless, the molecular rate  $\Lambda(T)$  for the HD target, which takes into account the deuteron motion within the molecule HD, is closer to the data than the nuclear rate  $\lambda(T)$ . From Fig. 12 one can conclude that the theoretical rate  $\Lambda(T)$ , which takes into account an appreciable isotopic effect, is closer to the experimental data (compare the rates for  $D_2$  and HD).

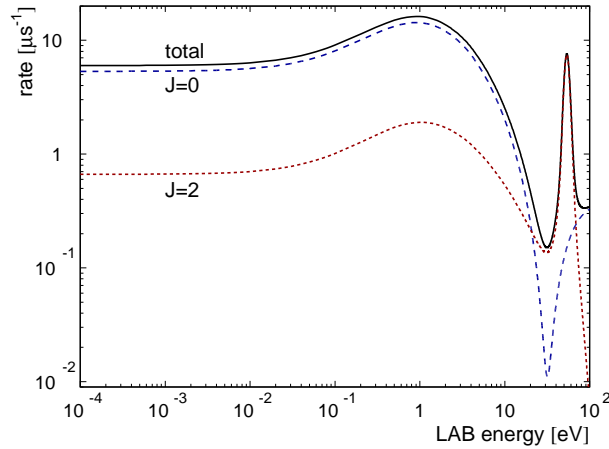


FIG. 13. (Color online) The contributions from the rotational states  $J = 0$  and  $2$  to the total molecular rate  $\Lambda(E)$  of nonresonant  $dt\mu$  formation in  $D_2$  at  $300$  K.

The contributions to the total rate  $\Lambda(E)$  from the nonresonant  $dt\mu$  formation in the rotational states  $J = 0$  and  $2$  are shown in Fig. 13 as functions of LAB energy. For the sake of clarity, a higher-energy contribution from the state  $J = v = 1$  of  $dt\mu$ , which is plotted in Fig. 10, is not included here. A negligible contribution from the state  $J = 1, v = 0$  of  $dt\mu$  is not visible in this plot. The presented rates have been calculated assuming the 300-K Boltzmann distribution of the rotational levels of the target  $D_2$  molecules.

Our calculations of the thermally-averaged molecular rates  $\Lambda(T)$  are summarized in Tables II and III. The rates for the rotational states  $K = 0, 1$  of target molecules at 30 K are

TABLE II. The calculated averaged nonresonant formation rates of muonic molecules [ $10^6 \text{ s}^{-1}$ ] for different populations of the rotational numbers  $K$  of the target hydrogenic molecules.

Muonic molecule	Target molecule	Temperature $T = 30 \text{ K}$			Temperature $T = 300 \text{ K}$ Boltzmann distribution
		$K = 0$	$K = 1$	Statistical	
$pp\mu$	$H_2$	1.806	1.805	1.805	1.799
$pd\mu$	$H_2$	5.626	5.618	5.620	5.582
$pt\mu$	$H_2$	6.375	6.363	6.366	6.317
$dd\mu$	$D_2$	0.0788	0.0829	0.0801	0.139
$dt\mu$	$D_2$	4.083	4.433	4.200	7.249
$tt\mu$	$T_2$	2.685	2.681	2.682	2.639

separately shown in Table II. The corresponding rate for the statistical mixture of these states is also given. These particular rates were calculated since at low temperatures the rotational

TABLE III. The calculated averaged nonresonant formation rates [ $10^6 \text{ s}^{-1}$ ] for different rotational numbers  $J$  of the muonic-molecule states  $Jv$ . The Boltzmann distribution of rotational states of the target molecules is assumed for the both temperatures.

Temperature [K]	State $J$	Muonic molecule (Target molecule)					
		$pp\mu$ ( $H_2$ )	$dd\mu$ ( $HD$ )	$dd\mu$ ( $D_2$ )	$dt\mu$ ( $D_2$ )	$dt\mu$ ( $DT$ )	$tt\mu$ ( $T_2$ )
30	0	0.008	0.0568	0.0653	3.655	3.893	0.003
	1	1.798	0.0119	0.0119	0.000	0.000	2.680
	2	—	0.0015	0.0019	0.454	0.484	0.000
	total	1.806	0.0702	0.0791	4.109	4.377	2.683
300	0	0.007	0.1170	0.1234	6.444	6.550	0.003
	1	1.792	0.0118	0.0118	0.000	0.000	2.636
	2	—	0.0038	0.0041	0.805	0.819	0.000
	total	1.799	0.1326	0.1393	7.249	7.369	2.639

levels of hydrogen-isotope molecules in certain experimental targets are not equilibrated according to the Boltzmann distribution. On the other hand, at  $T \gg 30 \text{ K}$ , many rotational levels of the target molecules are excited. They obey the Boltzmann distribution in typical experimental conditions. Therefore, this distribution was applied in the calculations of the formation rates for  $T = 300 \text{ K}$ . A significant difference of the average  $dt\mu$  formation rate in

the states  $K = 0$  and  $K = 1$  of  $D_2$  (see Table II) is due to a strong increase of the dominant nuclear formation rate  $J = 1 \rightarrow J = 0$  in the interval 0–0.1 eV and a greater internal kinetic energy of  $D_2$  in the state  $K = 1$ . The contributions from different rotational states  $J$  of the created muonic molecules to the total nonresonant formation rate  $\Lambda(T)$  are shown in Table III for 30 and 300 K. Here the Boltzmann distribution of the rotational levels of the target molecules is assumed for the both temperatures. One can see that the molecular rates  $\Lambda(T)$  of nonresonant  $dd\mu$  formation (in HD and  $D_2$ ) and  $dt\mu$  formation (in  $D_2$  and DT) display a significant isotope effect, in particular at the lower temperature.

The formation rates of muonic molecules, which were calculated and measured in various experiments, are compared in Table IV. Here the values of the rates from Refs. [1, 15] and

TABLE IV. Experimental and calculated rates [ $10^6 \text{ s}^{-1}$ ] of nonresonant formation of the muonic hydrogen molecules in different hydrogenic targets.

Muonic molecule	Experiment			Theory		
	Rate	Conditions	Ref.	Rate	Authors	Ref.
$pp\mu$	$0.6^{+0.8}_{-0.5}$	Gas, 300 K*	[30]	2.6	Zel'dovich and Gershtein	[1]
	$1.89 \pm 0.20$	Liquid, 22 K*	[31]	3.9	Cohen et al.	[15]
	$2.55 \pm 0.18$	Liquid, 22 K*	[32]	2.20	Ponomarev and Faifman	[16]
	$2.74 \pm 0.25$	Gas, 300 K*	[33]	1.80	Faifman	[17]
	$2.34 \pm 0.17$	Gas, 300 K*	[34]	1.81	Present work, 22 K	
	$3.21 \pm 0.24$	Solid, 3 K	[35]	1.80	Present work, 300 K	
	$2.01 \pm 0.09$	Gas, 300 K	[20]			
$pd\mu$				1.3	Zel'dovich and Gershtein	[1]
	$5.8 \pm 0.3$	Liquid, 22 K*	[31]	3.0	Cohen et al.	[15]
	$6.82 \pm 0.25$	Liquid, 22 K*	[32]	5.91	Ponomarev and Faifman	[16]
	$5.53 \pm 0.16$	Gas, 300 K*	[34]	5.63	Faifman	[17]
	$5.9 \pm 0.9$	Liquid, 22 K*	[36]	5.63	Present work, 22 K	
	$5.6 \pm 0.2$	Liquid, 22 K*	[37]	5.58	Present work, 300 K	
$pt\mu$				0.4	Zel'dovich and Gershtein	[1]
				6.49	Ponomarev and Faifman	[16]
	$7.5 \pm 1.3$	Liquid, 23 K*	[38]	6.38	Faifman	[17]
				6.38	Present work, 22 K	
				6.32	Present work, 300 K	
$tt\mu$				0.65	Zel'dovich and Gershtein	[1]
	$1.8 \pm 0.6$	Liquid, 23 K	[39]	2.96	Ponomarev and Faifman	[16]
	$2.3 \pm 0.6$	Solid, 16 K	[40]	2.64	Faifman	[17]
	$2.84 \pm 0.32$	Liquid, 22 K	[41]	2.69	Present work, 22 K	
				2.64	Present work, 300 K	

Refs. [16, 17] are quoted at collision energy near zero, and  $\varepsilon = 0.04$  eV, respectively. The value of  $\lambda_{pp\mu}$  from the work [15] has been corrected due to the updated value of the density of nuclei of liquid hydrogen  $N_0 = 4.25 \cdot 10^{22} \text{ cm}^{-3}$ , used in the present work, and in accordance with the remark of review [1], where is pointed out, that the corrected value should be two times less. The label “Present work” denotes the average rate for the 22-K or 300-K Maxwell

distribution of muonic-atom energies. The asterisk superscript denotes an assumed value, when the experimental temperature is not explicitly given in a corresponding reference. As can be seen from this table, for the majority of muonic molecules, the calculated rates are in good agreement with the experimental data. Only the value of  $pp\mu$  formation rate, which is topical due to the forthcoming experiments [8, 9], is a special case because of the disagreements between the theory and experiments. Moreover, the experimental data measured in different gaseous, liquid and solid hydrogen targets differ among themselves and are not sufficiently consistent. Therefore it is rather complicated to make a conclusion about the degree of agreement between the experimental and the theoretical values of the  $pp\mu$  formation rates.

## V. CONCLUSIONS

A role of the internal nuclear motion in the nonresonant formation of muonic hydrogenic molecules has been considered. In general, this motion leads to a significant smearing of the energy-dependent formation rates  $\Lambda(\varepsilon)$  in the  $a\mu + BX$  system, when the corresponding input rates  $\lambda(\varepsilon_b)$  calculated in the  $a\mu + b$  system [17] strongly change within the energy intervals comparable with the magnitude of vibrational quanta of the target molecules  $BX$  ( $\sim 0.1$  eV). In particular, this effect is important in the case of nonresonant  $dd\mu$  and  $dt\mu$  formation at  $\varepsilon \lesssim 0.1$  eV, which significantly affects the steady-state kinetics of  $\mu\text{CF}$  processes. Also, an appreciable isotopic effect in  $dd\mu$  nonresonant formation in  $\text{D}_2$  and HD gas has been found. Therefore, accurate simulations of various low-energy muonic processes in hydrogenic molecular targets require the use of the nonresonant formation rates with the nuclear-motion effect taken into account.

## ACKNOWLEDGMENTS

The authors are grateful to Prof. L. I. Men'shikov for helpful discussions.

- 
- [1] Ya. B. Zeldovich and S. S. Gershtein, Usp. Fiz. Nauk. **71**, 581 (1960), [Sov. Phys. Uspekhi **3**, 593 (1961)].
  - [2] L. I. Ponomarev, Contemp. Phys. **31**, 219 (1990).
  - [3] D. V. Balin, V. A. Ganzha, S. M. Kozlov, et al., Phys. Part. Nuclei **42**, 185 (2011).
  - [4] L. N. Bogdanova, D. L. Demin, V. N. Duginov, et al., Phys. El. Part. At. Nucl. Lett **9**, 605 (2012).
  - [5] L. N. Bogdanova, D. L. Demin, and V. V. Filchenkov, Yad. Fiz. **78**, 12 (2015), [Phys. At. Nucl. **78**, 10–19 (2015)].
  - [6] MuCap Collaboration, <http://muon.npl.washington.edu/exp/MuCap/>.
  - [7] MuSun Collaboration, <http://muon.npl.washington.edu/exp/MuSun/>.
  - [8] A. Adamczak, D. Bakalov, L. Stoychev, and A. Vacchi, Nucl. Instrum. Meth. B **281**, 72 (2012).
  - [9] R. Pohl, F. Nez, L. M. P. Fernandes, et al., JPS Conf. Proc. **18**, 011021 (2017).
  - [10] V. I. Korobov, I. V. Puzynin, and S. I. Vinitsky, Muon Catal. Fusion **7**, 63 (1992).
  - [11] V. I. Korobov, J. Phys. B **37**, 2331 (2004).

- [12] A. M. Frolov, Eur. Phys. J. D **66**, 212 (2012).
- [13] E. A. Vesman, Pis'ma Zh. Eksp. Teor. Fiz. **5**, 113 (1967), [JETP Lett. **5**, 91 (1967)].
- [14] L. I. Men'shikov, L. I. Ponomarev, T. A. Strizh, and M. P. Faifman, Zh. Eksp. Teor. Fiz. **92**, 1173 (1987), [Sov. Phys. JETP **65**, 656 (1987)].
- [15] S. Cohen, D. L. Judd, and R. J. Riddell, Jr., Phys. Rev. **119**, 397 (1960).
- [16] L. I. Ponomarev and M. P. Faifman, Zh. Eksp. Teor. Fiz. **71**, 1689 (1976), [Sov. Phys. JETP **44**, 886 (1976)].
- [17] M. P. Faifman, Muon Catal. Fusion **4**, 341 (1989).
- [18] A. Adamczak and M. P. Faifman, Hyperfine Interact. **209**, 63 (2012).
- [19] S. Knaack, Ph.D. thesis, UIUC (2012).
- [20] V. A. Andreev, T. I. Banks, R. M. Carey, et al., Phys. Rev. C **91**, 055502 (2015).
- [21] A. Adamczak and M. P. Faifman, Eur. Phys. J. D **51**, 341 (2009).
- [22] M. P. Faifman, L. I. Men'shikov, and T. A. Strizh, Muon Catal. Fusion **4**, 1 (1989).
- [23] Yu. V. Petrov, V. Yu. Petrov, and H. H. Schmidt, Phys. Lett. B **331**, 266 (1994).
- [24] L. D. Landau and E. M. Lifshitz, Quantum Mechanics. Nonrelativistic Theory (Nauka, Moscow, 1989), (in Russian).
- [25] C. K. Raju, J. Phys. A: Math. Gen. **15**, 381 (1982).
- [26] A. Adamczak, Phys. Rev. A **74**, 042718 (2006).
- [27] M. Abramowitz and I. A. Stegun, Handbook of Mathematical Functions (Dover Publications, New York, 1970).
- [28] L. I. Ponomarev, I. V. Puzynin, and T. P. Puzynina, Preprint JINR, P4-9183, Dubna (1975), (in Russian).
- [29] M. Bubak and M. P. Faifman, Preprint JINR, E4-87-464, Dubna (1987).
- [30] V. P. Dzhelepov, P. F. Ermolov, Yu. A. Kushnirenko, et al., Zh. Eksp. Teor. Fiz. **42**, 439 (1962), [Sov. Phys. JETP **15**, 306 (1962)].
- [31] E. J. Bleser, E. W. Anderson, L. M. Lederman, et al., Phys. Rev. **132**, 2679 (1963).
- [32] G. Conforto, C. Rubbia, E. Zavattini, and S. Focardi, Nuovo Cimento **33**, 1001 (1964).
- [33] Yu. G. Budyashov, P. F. Yermolov, A. D. Konin, et al., Preprint JINR, R15-3964, Dubna (1968).
- [34] V. M. Bystritski, V. P. Dzhelepov, V. I. Petrukhin, et al., Zh. Eksp. Teor. Fiz. **71**, 1680 (1976), [Sov. Phys. JETP **44**, 881 (1976)].
- [35] F. Mulhauser, J. L. Beveridge, G. M. Marshall, et al., Phys. Rev. A **53**, 3069 (1996).
- [36] W. H. Bertl, W. H. Breunlich, P. Kammel, et al., Atomkernenergie-Kerntechnik **43**, 184 (1983).
- [37] C. Petitjean, K. Lou, P. Ackerbauer, et al., Muon Catal. Fusion **5/6**, 199 (1990/91).
- [38] P. Baumann, H. Daniel, S. Grunewald, et al., Phys. Rev. Lett. **70**, 3720 (1993).
- [39] W. H. Breunlich, M. Cargnelli, P. Kammel, et al., Muon Catal. Fusion **1**, 121 (1987).
- [40] T. Matsuzaki, K. Nagamine, K. Ishida, et al., Hyperfine Interact. **118**, 229 (1999).
- [41] L. N. Bogdanova, V. R. Bom, A. M. Demin, et al., Zh. Eksp. Teor. Fiz. **135**, 242 (2009), [JETP **108**, 216 (2009)].